



CHORUS

This is the accepted manuscript made available via CHORUS. The article has been published as:

Unexpected high inelastic phonon transport across solid-solid interface: Modal nonequilibrium molecular dynamics simulations and Landauer analysis

Tianli Feng, Yang Zhong, Jingjing Shi, and Xiulin Ruan

Phys. Rev. B **99**, 045301 — Published 7 January 2019

DOI: [10.1103/PhysRevB.99.045301](https://doi.org/10.1103/PhysRevB.99.045301)

Unexpected high inelastic phonon transport across solid-solid interface: Modal nonequilibrium molecular dynamics simulations and Landauer analysis

Tianli Feng,¹ Yang Zhong,¹ Jingjing Shi,¹ and Xiulin Ruan^{1,*}

¹*School of Mechanical Engineering and the Birck Nanotechnology Center,
Purdue University, West Lafayette, Indiana 47907-2088, USA*

(Dated: November 12, 2018)

As a crucial part in thermal management, interfacial thermal transport is still not well understood. In this paper, we employ the newly developed modal nonequilibrium molecular dynamics to study the Si/Ge interfacial thermal transport and clarify several long-standing issues. We find that the few atomic layers at the interface are dominated by interfacial modes, which act as a bridge that connects the bulk Si and Ge modes. Such bridging effect boosts the inelastic transport to contribute more than 50% to the total thermal conductance even at room temperature. The apparent inelastic transport can even allow effective four-phonon processes across the interface when the mass difference between the two materials is large. Surprisingly, optical phonon modes can contribute equal or more thermal conductance than the acoustic modes due to the bridging effect. From the modal temperature analysis, we find that the phonon modes are in strong thermal nonequilibrium near the interface, which impedes the thermal transport. The widely used Landauer approach that does not consider the phonon nonequilibrium can lead to inaccurate results. We have modified the Landauer approach to include the inelastic transmission and modal thermal nonequilibrium. The approach is used to analyze our modal NEMD results, and the mode-dependent phonon transmission function that includes inelastic scattering has been derived. Our results unveil the fundamental thermal transport physics across interfaces and will shed light on the future engineering in thermal management. It provides a method of calculating modal phonon transmission functions that includes inelastic scattering from molecular dynamics.

I. INTRODUCTION

Interfaces between dissimilar materials can impede heat transfer and create thermal resistance and heat accumulation. Managing heat flow across material interfaces has become a major challenge for improving the performance of current devices ranging from large-scale engines^{1,2}, personal electronics³ to microprocessor chips and nanoscale transistors⁴. In recent years, great effort has been spent on improving the heat transport between dissimilar materials⁵⁻⁸. To date, the underlying fundamental physical properties that dominate the interfacial heat flow are, however, still poorly understood. A deeper knowledge and better understanding of these properties are, therefore, highly demanded for gaining better control on the thermal flow and improving energy efficiency of devices.

The interfacial thermal transport can be characterized by the thermal resistance R or its reciprocal, thermal conductance G , which is the heat flow rate Q divided by the temperature jump ΔT at the interface. The interfacial thermal resistance is induced by the blocking and scattering of heat carriers at the interfaces. In most dielectrics and semiconductors, the dominant heat carrier is phonon, which is a quantization of lattice vibrations. The transmission of phonon across interfaces can be divided into two categories: elastic and inelastic transport, which are determined by whether the phonon frequency changes or not after the transmission. To quantify the elastic and inelastic transport, phonon analysis on the spectral (frequency) or modal level is required. A lot of methods have been proposed to calculate the spectral phonon conductance such as the acoustic mismatch model (AMM)⁹, diffuse mismatch model (DMM)^{10,11} and atomistic Green's function (AGF)¹²⁻¹⁵. These methods, however, assume elastic phonon transport and neglect the inelastic part. Although some works¹⁶⁻²³ have im-

proved these methods to incorporate the inelastic contribution, they are interpretive rather than predictive tools. The wave-packet method²⁴⁻²⁸ also largely only capture elastic transport.

Great progress based on molecular dynamics (MD) simulations has been made in recent few years in the full prediction of phonon modal interfacial thermal conductance²⁹⁻³⁸. MD simulation naturally includes all the orders of lattice anharmonicity. All these works²⁹⁻³⁸ using equilibrium MD and nonequilibrium MD are based on the energy exchange rate formalism between materials A and B. A more general formula to include the three and many-body interactions is^{29,36-38}

$$Q_{A \rightarrow B} = - \sum_{i \in A} \sum_{j \in B} \left\{ \frac{\mathbf{p}_i}{m_i} \frac{-\partial H_j}{\partial \mathbf{r}_i} + \frac{\mathbf{p}_j}{m_j} \frac{-\partial H_i}{\partial \mathbf{r}_j} \right\}, \quad (1)$$

where i and j label the atoms in materials A and B. H , \mathbf{p} , \mathbf{r} and m are the individual Hamiltonian, momentum, position and mass, respectively. If only pairwise interactions are present, it can be wrote as^{39,40}

$$Q_{A \rightarrow B} = -\frac{1}{2} \sum_{i \in A} \sum_{j \in B} \mathbf{F}_{ij} \cdot (\dot{\mathbf{u}}_i + \dot{\mathbf{u}}_j), \quad (2)$$

where \mathbf{F}_{ij} is the interatomic force between the atoms i and j . $\dot{\mathbf{u}}_i$ and $\dot{\mathbf{u}}_j$ are the velocities of the atoms in A and B, respectively. Based on the energy exchange rate formalism, these works²⁹⁻³⁸ can be divided into two categories depending on whether they are on the frequency or modal level.

On the frequency level, a most widely used method was developed by Volz *et al.*^{31,32}. They decomposed the spectral conductance into elastic and inelastic contributions by decomposing the force \mathbf{F} into different orders $\mathbf{F} = \mathbf{F}^{(2)}\mathbf{u} + \mathbf{F}^{(3)}\mathbf{u}\mathbf{u}/3 + \dots$. The second-order term is responsible for the elastic conductance while the third and higher orders inelastic. This method

has also been used successfully in other work³⁵ and then been extended by Zhou and Hu³³ for a full quantification of the inelastic contribution. Despite the great success of these methods, they cannot distinguish interfacial modes from bulk modes. Moreover, they are on the frequency while not on the modal level³³ and they cannot calculate the mode contributions to the conductance. Some results could not match with nonequilibrium molecular dynamics (NEMD) simulations, and the discrepancy was attributed to the existence of interfacial modes^{29–32}.

On the modal level, considerable progress has been made by Volz *et al.*^{29,30,41} and Gordiz and Henry³⁶. By decomposing the velocity $\dot{\mathbf{u}}$ in Eq.(1) or (2) into normal modes, they obtained the “mode-to-mode” thermal conductance $G_{nn'}$. Although this method has also been successfully used in other work³⁴, the modal conductance is not from a mode of A to a mode of B. Instead, it is from a combined mode of A and B to another combined mode of A and B. The physical meanings of the modes n and n' and their conductance $G_{nn'}$ are, therefore, unclear. A limitation of this method is that it decomposes the interfacial atoms’ vibration by using bulk phonon normal modes. It will be seen later in this paper that the interfacial atoms vibrate significantly differently from bulk modes. Realizing this limitation, Gordiz and Henry have introduced the idea of interfacial modes in their model^{37,38}.

Another important issue existing in some of these works is the usage of equilibrium molecular dynamics (EMD). EMD has two critical issues in the study of interfacial thermal transport. 1) The whole system is in thermal equilibrium, which cannot reproduce the natural state of nonequilibrium phonon distribution near interfaces⁴². 2) EMD simulations often assume periodic boundary condition along the heat flow direction. This condition makes the system as a superlattice, the heat transfer in which is, however, significantly different from that across single interface. Large portion of phonons might transport coherent through superlattice interfaces⁴³.

To avoid these limitations and gain insight into the modal heat conduction contribution across interfaces, in the present paper we employ NEMD simulations with the time domain direct decomposition method (TDDDM) developed for bulk materials by Zhou and Hu⁴⁴ to study the thermal transport across interfaces. *This method does not rely on Eq.(1) or (2)*. The system near interface can be divided into three regions: left near-interface region, middle interface region, and right near-interface region. The methods based on Eq.(1) or (2) discussed above limit the studies to the inside of the middle interface region, which does not contain the information of how the phonons come from left and leave for the right (assuming heat flows from left to right). In the present paper, we show that the middle interface region is so thin that it can be viewed as “interface”, and the phonons are transport from the bulk modes of A through the “interface” to the bulk modes of B.

The remaining of the paper is organized as follows. In Sec.II, we first choose proper materials and interatomic potentials for the simulations (II A), and then we determine a simulation domain size so that it does not have size effect on the interfacial transport (II B). After that, we calculate phonon densities of states of the atoms in different regions ranging

from the left end, through the interface, to the right end (II C). By doing so, we can figure out which regions are dominated by interfacial or bulk modes. For the regions that are dominated by bulk modes, we employ the TDDDM method to decompose the thermal conductance to every phonon mode. The formalism is presented in Sec.II D. The results are presented in Sec.III. In Sec.III A, we study the interfacial modal transport for interfaces with different mass ratios (²⁸Si/⁷³Ge, ⁶Si/⁷³Ge and ²Si/⁷³Ge) to investigate the heat conductance contribution of the three-, four- and higher-orders of phonon scattering. To study the temperature effect on the inelastic transport, three different temperatures 20, 300, and 1000K are studied. In Sec.III B, phonon modal temperatures are calculated, and the thermal nonequilibrium near interface is discussed. In Sec.III C, we compare our NEMD results with AMM and DMM models, which assume thermal equilibrium and consider elastic transport only. We have modified the Landauer approach to include the inelastic transport and the modal thermal non-equilibrium. In Sec.III D, we repeat the modal analysis for a smaller size to make sure size effect is small. To examine if the elastic and inelastic heat transport is reversible, we flipped the heat source and sink and repeat the work. In Sec.IV, conclusions are drawn.

II. SIMULATION AND METHODOLOGY

The MD simulations were performed using the LAMMPS package⁴⁵ with the Tersoff interatomic potential^{46,47}. The lattice constant $a_{Si} = 5.442 \text{ \AA}$ at room temperature is obtained by relaxing the atomic structures in MD. The time step for simulations is set as 1 fs which is short enough to resolve all the phonon modes. The two ends of the systems are fixed during the simulations as shown in Fig. 1. We first relax the geometries under constant pressure and temperature (NPT) for 10 ns (10 million time steps), and then change the ensemble to constant energy and temperature (NVE) except for the fix boundaries for another 20 ns (20 million time steps). In the NVE ensemble, we apply the temperature differences on the two reservoirs using the Langevin thermostat and stabilize the heat current as well as temperature gradient for 10 ns. The next 10 ns simulations are used to extract the atomic velocities to do normal mode analysis. These setups are found to be able to give stable results. The entire simulation domain is divided into many cells, and modal decomposition is done separately for each cell. One such cell is the sample volume drawn in Fig. 1, which indicates that the atoms in that volume are used to calculate the phonon modal heat flux (and temperature) at that location. The sample volume generally contains $8 \times 8 \times 8$ conventional cells with 4096 atoms. To study a subtler spatial distribution, a smaller sample volume can be used. Periodic boundary conditions are applied to the lateral directions to model infinite large dimensions. The temperatures applied on the two reservoirs are $\pm 30 \text{ K}$ on the averaged temperature. The damping parameter specified in time units determines how rapidly the temperature is relaxed in the reservoir⁴⁸. In our simulation, it is set as 0.5 ps, which is suitable for a stable heat current. It can vary to some extent but not too much.

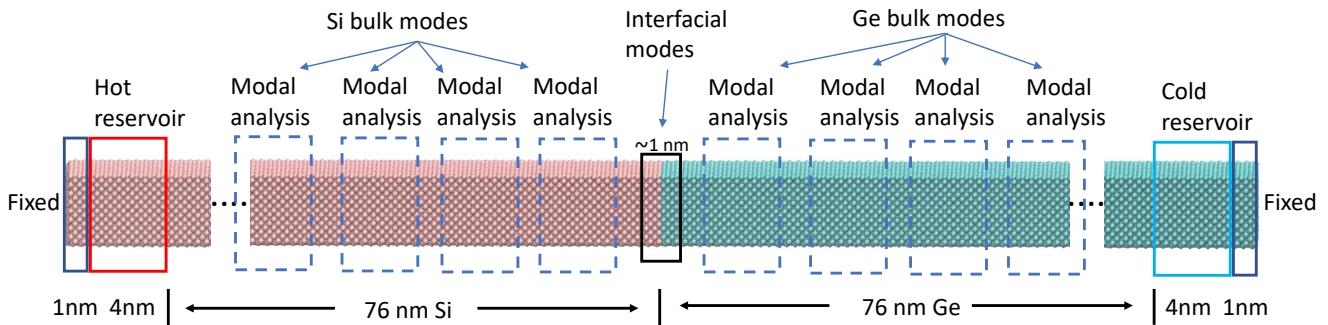


FIG. 1: NEMD simulation setup. The left and right edges are fixed during simulations. Total length of each side is 76 nm. The lateral dimensions are 8×8 conventional cells (4.4×4.4 nm), with periodic boundary conditions applied. Modal analyses are done at different locations throughout the domain.

A damping parameter that is too short (e.g. < 0.01 ps) may lead to unstable temperature profile, while a too long damping parameter (e.g. > 10 ps) is not able to build up a suitable temperature gradient. Different temperature differences, heat reservoir damping parameters, and two-end boundary conditions have been tried in our benchmark process, and the conclusions are the same.

A. Choose proper simulation materials: eliminate strain

Ar/heavy-Ar and Si/Ge interfaces are the most common systems for the study of fundamental phonon transport^{29–38}. Here we do not choose argon since it does not have optical phonon branches, which are important for the study of inelastic phonon transport. Besides, Si/Ge interfaces are of great significance in semiconductor industry and thermoelectrics^{14,15,26,49–53}.

Si and Ge have a lattice mismatch, e.g., the lattice constants are $a_{Si} = 5.431$ and $a_{Ge} = 5.658$ Å experimentally⁵⁴ or 5.442 and 5.678 Å using Tersoff potential^{46,47} relaxed at 300K, respectively. MD simulations are hard to simulate the mismatched interface between Si/Ge since it requires a large cross-section area to fit both a_{Si} and a_{Ge} . Therefore, two methods have been employed in literature to overcome this difficulty in simulations: 1) taking the average lattice constant $a = (a_{Si} + a_{Ge})/2$ for the interface cross-section to enforce the lattice to match with each other; 2) changing the interatomic potential of Ge to be the same as Si so that they have the same lattice constant. In both methods, periodic boundary conditions (P.B.C.) are applied on the lateral directions to mimic unconfined interface. We have found that the first one can induce a large artificial strain, which makes the interface vibrate around the center with a large amplitude as seen in the video in the supplemental materials⁵⁵. Moreover, the atom positions can deviate a few nanometers (more than 10 times of lattice constant) from its equilibrium if the simulation system is long. Although the NEMD temperature profile obtained from the first method is still in a good shape owing to long-time averaging, the phonon modal analysis does not work well since it relies strongly on the atomic positions and velocities near their equilibrium. Therefore, we choose the second method in this

paper. Using the second method, we indeed observed that the system is stable with atoms vibrating near their equilibrium positions (See the video in supplemental materials⁵⁵), and it will be seen that the phonon modal analysis work excellently.

B. Size effect: determine simulation size

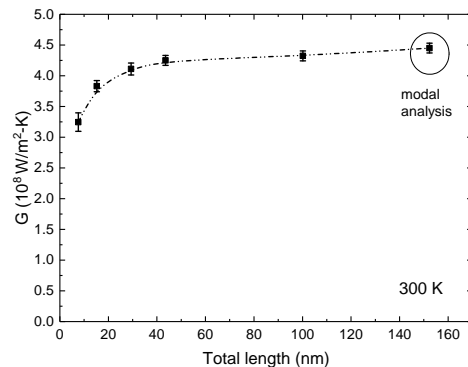


FIG. 2: The domain size-dependent thermal conductance $G = Q_{MD}/\Delta T_{MD}$ obtained from NEMD simulations at 300 K.

Heat reservoirs may affect the interfacial thermal conductance by reflecting the transmitted phonons back through interface if the length of the simulation domain is short⁵⁶. Liang *et al.* has proposed a method to effectively eliminate such a size effect by using rough reservoir boundaries which reflect the phonons diffusely and therefore, they do not travel back to across interface⁵⁶. The size-dependent thermal conductance G of Si/Ge interface obtained from NEMD simulations is shown in Fig.2. It is seen that G nearly converges at 152 nm. To make sure this, we have used roughened reservoir boundaries and found that G does not change much. Therefore, the results in the remaining of this paper were obtained by using 152 nm-simulation domain except special note.

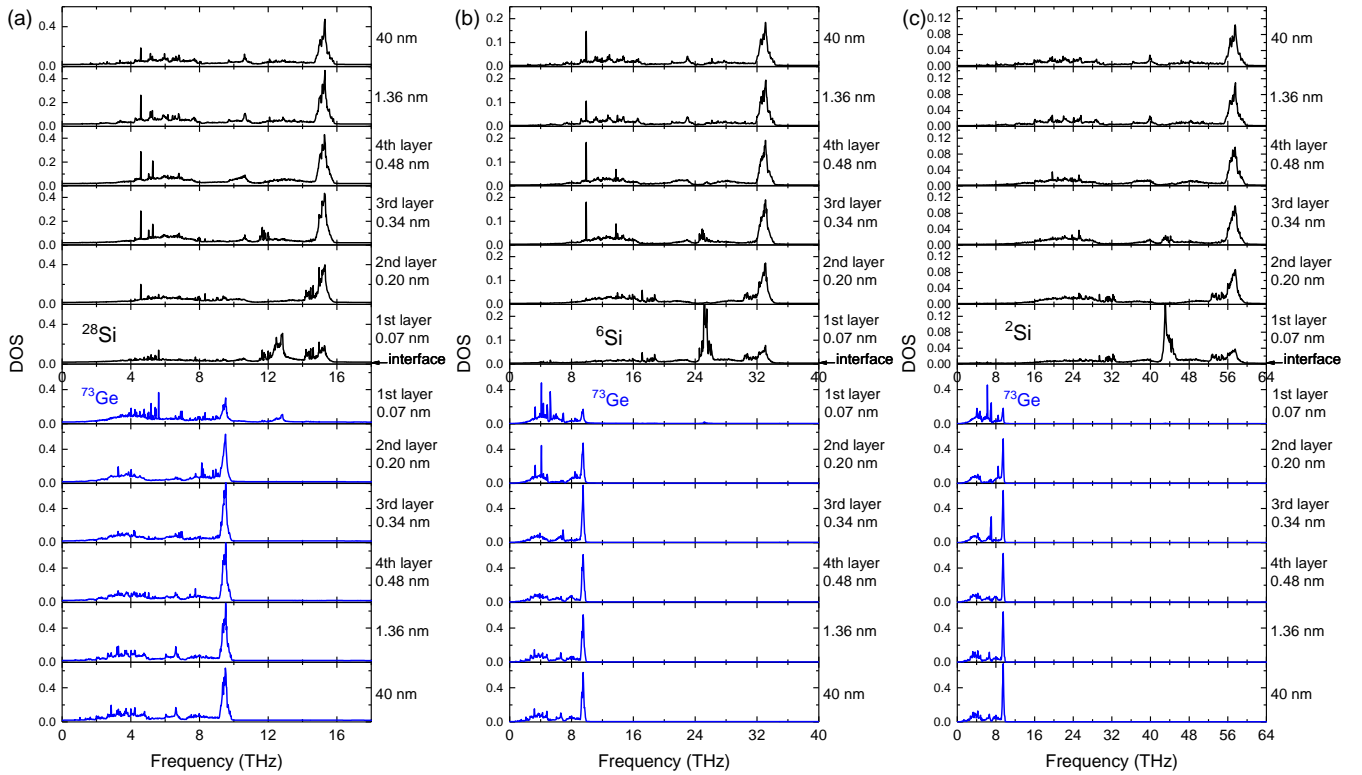


FIG. 3: Phonon densities of states (DOS) at different locations throughout the domain for the interfaces (a) $^{28}\text{Si}/^{73}\text{Ge}$, (b) $^6\text{Si}/^{73}\text{Ge}$ and (c) $^2\text{Si}/^{73}\text{Ge}$. In each subfigure, the top four panels are Si and the bottom four panels are Ge. Each panel is the DOS of the atoms at certain location with the distance from the interface labeled on the right of each panel.

C. Phonon DOS: Determine interfacial and bulk regions

Before doing modal analysis of any region of the system, we need to determine if that region is governed by bulk modes or interfacial modes since the TDDDM method relies on phonon eigenvectors. As indicated by Gordiz and Henry^{37,38}, the phonon modes near interface are different from the bulk modes. In Fig.3 (a), we have shown the densities of states extracted by using the Fourier transform of the atomic velocity autocorrelations in different regions in our NEMD simulations. It is seen that the atomic layer nearest to interface has significantly different phonon modes with bulk modes. These interfacial modes are, however, mostly terminated at the third nearest layer, which is only 0.3 nm away from interface. Therefore, the most significant interfacial region is about 0.6 nm thick. If this thin region is taken as "interface", the interfacial thermal transport can be viewed as the bulk modes of Si to the bulk modes of Ge through the "interface". Inside this "interface" are numerous phonon modes conversions and redistributions.

Note that the "interfacial region" cannot be definitely defined, and it depends on phonon modes. The modal vibration eigenvectors can be affected by the interface that is wavelength-long away. The interfacial region thicknesses are different for different phonons. Gordiz and Henry³⁷ have used eigenvectors to identify the interfacial region. The eigenvectors depend on the second order force constant as well as the wavelength

of the mode. For the Tersoff potential used in our system, the cutoff radius for interatomic forces is only to the nearest neighbors, and the interfacial region is thin. For other potentials such as Lennard-Jones³⁷, the cutoff radius might be longer and the interfacial region might be thicker. For the very-long wavelength phonons (for example 200 Å), the interface can affect them even when they are 200 Å away from the interface. However, these long wavelength phonons have extremely low DOS and contribute little to thermal transport. For example, a $16 \times 16 \times 16$ \mathbf{k} -grid is fine enough to get a good thermal conductivity value for silicon⁵⁷, and the longest wavelength along x direction using this \mathbf{k} -grid is around 4 nm. In our work we use a $16 \times 16 \times 16$ \mathbf{k} -grid and we choose 8 unit cells away from the interface to decompose the modes so that we can use the bulk modes and eigenvectors to do decomposition. This is right the difference between this work and the literature²⁹⁻³⁸.

The literature focused on the intermediate state of the thin interfacial region while our work focuses on the initial and final states. Introducing an extra interfacial region and decompose the heat flux inside this region to the interfacial modes with our modal NEMD method will bring several challenges as listed below.

1. The thermal transport problem becomes: $A \rightarrow C \rightarrow B$ (for convenience, we label the interfacial region as C). Then the interfaces of this system become A/C interface and C/B interface while C is a new material. Therefore, the modal analysis will not give a temperature jump inside C. Instead, it

will give temperature jumps at these two new interfaces A/C and C/B. This is inconsistent with the NEMD results that the temperature jump occurs at the original interface inside C, rather than at the two new interfaces.

2. Because two new interfaces are introduced, we need to consider the two more new interfacial regions, i.e., A/C interfacial region, C/B interfacial regions. If we label them as D and E respectively, we need to study the thermal transport for $A \rightarrow D \rightarrow C \rightarrow E \rightarrow B$. Then, we introduce two new interfaces again, i.e., between A and D, and between E and B. There will be numerous new interfacial regions that will be introduced. Therefore, it makes the study of the interfacial thermal transport extremely more complicated.

3. If C is regarded as a new material and the modal analysis is done inside this new material, as done in literature^{37,38}, the question becomes “how does a mode of C transfer its heat to another mode of C?” and “what is the transmission coefficient from a mode of C to another mode of C?”. Moreover, the modal conductance was calculated using the interfacial modal heat flux over the overall temperature jump at the original interface rather than the modal temperature jump. This treatment brings this inherent inconsistency, and the physical meanings of these questions are not very clear. For example, the transmission coefficient $\mathcal{T}_{\text{Ge} \rightarrow \text{Si}}(\omega_{\text{Ge}})$ for the $\text{Ge} \rightarrow \text{Si}$ heat flow should be a function of $0 < \omega < 10$ THz that describes the transmission of the modes of Ge, while the transmission coefficient $\mathcal{T}_{\text{Si} \rightarrow \text{Ge}}(\omega_{\text{Si}})$ for the $\text{Si} \rightarrow \text{Ge}$ heat flow should be a function of $0 < \omega < 16$ THz that describes the transmission of the modes of Si. However, the literature mixes them together and presents a single function $\mathcal{T}_{\text{Ge/Si}}(\omega)$ with $0 < \omega < 16$ THz for both cases. The physical meaning of that function is not very clear since the ω in that function is the frequency of the mixed mode of A&B as a single material (C). In other words, their results could not tell how much the phonon in Si with ω_{Si} is transmitted to Ge when heat flow is applied from Si to Ge, or how much the phonon in Ge with ω_{Ge} is transmitted to Si when heat flow is applied from Ge to Si. Instead, what they calculated is how much the phonon mode ω of Si&Ge together as a single material is transmitted to another phonon mode ω' . Moreover, including Ge when judging the percentage of inelastic contribution to the interfacial conductance will under-estimate the inelastic contribution, since the heat flux carried by 10 to 16 THz phonons is diluted. The more the Ge atoms are included in the interfacial region, the more under-estimation it will cause. This is why our approach gives higher inelastic contribution, as we will see.

Due to these challenges of using our modal NEMD method on the interface modes, we decided to use our method on the bulk modes, where we were able to decompose both heat flux and temperature jump.

We note that for the first layer of Ge, the high frequency DOS exists for $^{28}\text{Si}/^{73}\text{Ge}$ structure at around 13 THz, however, it becomes very small for $^6\text{Si}/^{73}\text{Ge}$ (at around 25 THz) and even disappears in $^2\text{Si}/^{73}\text{Ge}$. This is because of the resonance effect. When mass difference is small, the lighter-mass atoms can pull the heavier-mass atoms for faster vibration. As the mass difference becomes very large, the heavier-mass atoms cannot respond to the ultrafast vibration of the lighter atoms anymore.

In comparison, the low frequency DOS is still affected by each other.

D. Modal decomposition formalisms

For the bulk regions, we extract the phonon modal heat flux and temperature from NEMD simulations based on bulk eigenvectors. The real-space total heat flux can be converted and decomposed into phase-space phonon modal heat fluxes \mathbf{Q}_λ as developed by Zhou and Hu⁴⁴:

$$\mathbf{Q}_\lambda = \sum_{l,b}^{N_c,n} \left\langle \frac{1}{\sqrt{N_c m_b}} [E_{l,b}(t) - \mathbf{S}_{l,b}(t)] \mathbf{e}_{b,\lambda} \exp(i\mathbf{k} \cdot \mathbf{r}_{l,b}^0) \dot{\Phi}_\lambda(t) \right\rangle, \quad (3)$$

where $\dot{\Phi}_\lambda(t)$ is the time derivative of normal mode amplitude⁵⁸:

$$\dot{\Phi}_\lambda(t) = \frac{1}{\sqrt{N_c}} \sum_{l,b}^{N_c,n} \sqrt{m_b} \exp(-i\mathbf{k} \cdot \mathbf{r}_{l,b}^0) \mathbf{e}_{b,\lambda}^* \cdot \dot{\mathbf{u}}_{l,b}(t), \quad (4)$$

which is the connection between real-space atomic vibration to phase-space phonon mode. In Eq.(3), \mathbf{Q} is a vector, pointing towards the direction of heat flow. In our simulations, the heat flow is one-dimensional along the x direction, and in the remaining of this paper we use scalar Q instead. The subscript λ stands for a phonon mode (\mathbf{k}, ν) with \mathbf{k} and ν representing the phonon wave vector and dispersion branch, respectively. $\langle \rangle$ denotes the time average. Here, $E_{l,b}$ and $\mathbf{S}_{l,b}$ are the total energy and stress of the atom (l, b), respectively. l and b label the indices of the primitive cells and basis atoms with the total numbers represented by N_c and n , respectively. m, \mathbf{r} , and $\dot{\mathbf{u}}$ are the mass, equilibrium position, and velocity vector, respectively. $\mathbf{e}_{b,\lambda}$ and $\mathbf{e}_{b,\lambda}^*$ are the eigenvector component and its complex conjugate at the basis b for the mode λ , respectively. If the decomposition is done correctly, the summation of heat flux of all phonon modes should be equal to the heat flux obtained from real-space in MD simulations Q_{MD} :

$$\frac{1}{N_{\mathbf{k}}} \sum_{\lambda}^{3nN_{\mathbf{k}}} Q_\lambda = \frac{1}{N_c} Q_{MD}, \quad (5)$$

where $N_{\mathbf{k}}$ is the total number of \mathbf{k} points. Usually, we take $N_{\mathbf{k}} = N_c$.

With the modal heat flux Q_λ , the modal interfacial heat conductance can be derived by

$$G_\lambda = \frac{Q_\lambda}{\Delta T_{MD}}, \quad (6)$$

where ΔT_{MD} is the overall temperature drop at the interface in MD simulations. Although different phonons have different modal temperatures T_λ , the calculation of G requires the usage of overall temperature drop ΔT_{MD} rather than modal temperature drop ΔT_λ since experiment measures the apparent thermal conductance.

The real space overall temperature can also be converted and decomposed into the phonon modal temperatures T_λ as

developed by Feng *et al.*⁴²:

$$T_\lambda = \frac{1}{k_B} \langle \dot{\Phi}_\lambda^*(t) \dot{\Phi}_\lambda(t) \rangle, \quad (7)$$

where k_B is the Boltzmann constant.

In the formalisms, the only input is the real-space trajectory of the atoms in the sampled domains obtained from NEMD simulations. To eliminate the fluctuation in MD, Eqs.(3) and (7) need to be averaged over a sufficiently long time.

We limit our calculations to classical molecular dynamics, which assumes classical thermostat. To account for the quantum effect, a strict way is to use the MD simulations with quantum thermostat as been done by Ref.⁵⁹, but issues still exists⁵⁹. Instead, some works^{60,61} used a quantum correction to correct the temperature and the corresponding heat capacity or scattering rates. Since the quantum correction is still controversial in accounting for the quantum effect⁶⁰, and Gordiz and Henry³⁸ have shown that its effect on the interfacial thermal conductance is small, we do not consider quantum correction in this work.

III. RESULTS

A. Large inelastic transport

In Fig.4(a), the heat fluxes carried by different phonon modes in ²⁸Si and ⁷³Ge across their interface are plotted as a function of phonon frequency. The contribution of each phonon mode in the full BZ to the total thermal conductance G can be clearly read. The frequency-dependent accumulation of G is shown in Fig.4(c) top panel. The total conductance $G_{ph} = \sum_\lambda G_\lambda$ summed from the modal contributions in the full BZ is 4.5×10^8 W/m²-K, which agrees excellently with the conductance $G = Q_{MD}/\Delta T_{MD}$ calculated from real space as indicated by the dash line, where Q_{MD} is rate of the energy injected in the hot reservoir or extracted from the cold reservoir. This indicates that our modal analysis has accurately decomposed the MD heat flux to each phonon mode. Surprisingly, we find that the phonons in ²⁸Si with frequency higher than the ⁷³Ge cutoff frequency (10 THz) contribute 45% to G . In other words, the inelastic scattering contributes at least 45% to G . Such large inelastic contribution has never been discovered before because their studies were limited to the few interfacial atomic layers²⁹⁻³⁸, whose DOS is significantly different from bulk counterpart. With our results, it is seen that the high-frequency (optical) phonons in ²⁸Si dump their energy to the interfacial modes at the (~ 0.6 nm thick) interface region with frequency around 12 THz (as seen in the interfacial DOS) and then transfer it to the low-frequency phonons in ⁷³Ge. The phonons at the interface with frequency around 12 THz are important to bridge the thermal transport from Si to Ge, as discussed in Ref.^{29,33,36}. The existence of the interfacial region significantly facilitates the inelastic transport across interface. Its existence also makes the inelastic transport hard to be described by simple phonon-phonon scattering model, e.g., the commonly used three-phonon process. Zhou

and Hu³³ have found that the anharmonic scattering contribute 27% at room temperature with the three-phonon and higher orders contributing 17% and 10%, respectively. Their interface, however, has strain. Moreover, the interfacial modes are not considered in their method.

To examine how effectively the interfacial region facilitate the thermal transport across high-dissimilar materials, we have studied the Si/Ge interface with large mass difference by changing the Si mass to 6 or 2 a.u. The decomposed modal heat fluxes across ⁶Si/⁷³Ge are shown in Fig.4(b). Although a lot of phonons' heat fluxes are around zero with large error bars, the summation agrees with the conductance $G = Q_{MD}/\Delta T_{MD}$ calculated from real space as indicated by the dashed line in Fig.4(d). This indicates that the modal conductances are decomposed well statistically, despite the large MD fluctuation for individual modes. The total conductance G is significantly reduced to 0.8×10^8 W/m²-K as compared to ²⁸Si/⁷³Ge. Surprisingly, we find that the relative inelastic contribution does not change much. The phonons in ⁶Si with the frequency higher than the ⁷³Ge cutoff frequency (10 THz) still contribute around 40% to G even though their energy can be 3 times higher. This indicates that the interfacial region can bridge the phonons with significantly different energies as found by Gordiz and Henry^{37,38}. In terms of phonon-phonon scattering model, due to energy conservation law of scatterings, the phonons in ⁶Si above 32 THz must transfer their heat to the phonons in ⁷³Ge with maximum 10 THz by four-phonon and five-phonon processes (for example, 32 THz \rightarrow 10+10+10+2 THz).

The temperature effect is examined as shown in Fig.5. It is generally believed that decreasing temperature can largely reduce the inelastic phonon transport⁶². In our simulations, however, we find that the relative contribution of inelastic transport at 20 K is still as high as 40% owing to the bridging effect of interfacial modes^{37,38}.

To gain deeper insight into the modal thermal conductance, we have calculated the spectral $G(\omega)$, which is the differential of the cumulative G with respect to frequency. Surprisingly, we find that the overall shape of the spectral $G(\omega)$ follows the shape of DOS. The optical phonon has a sharp peak while the acoustic phonon shows a mild slop only. Overall, the optical and acoustic phonons contribute nearly 50% each. This is significantly different from the spectral thermal conductivity in homogeneous materials, which shows a sharp peak at the low-frequency acoustic phonon region while a tiny peak for the optical phonon, and the acoustic and optical phonons contribute $>80\%$ and $<20\%$, respectively⁶³. Such large difference is made by the interface, which plays a role of filter that redistribute the significance of different phonons. Another important finding is that the spectral heat fluxes (or conductances $G(\omega)$) of Si and Ge overlap with each other in the range of 0~5 THz, although their DOS's have a large difference in this frequency range. The spectral heat flux overlap indicates that the thermal transport in this frequency range is elastic.

By using the modal decomposition method, we are able to resolve phonon branch contributions to the interfacial thermal conductance, which could not be done in previous works²⁹⁻³⁸. As shown in Figs.4 and 5, the modal heat conductance (or heat

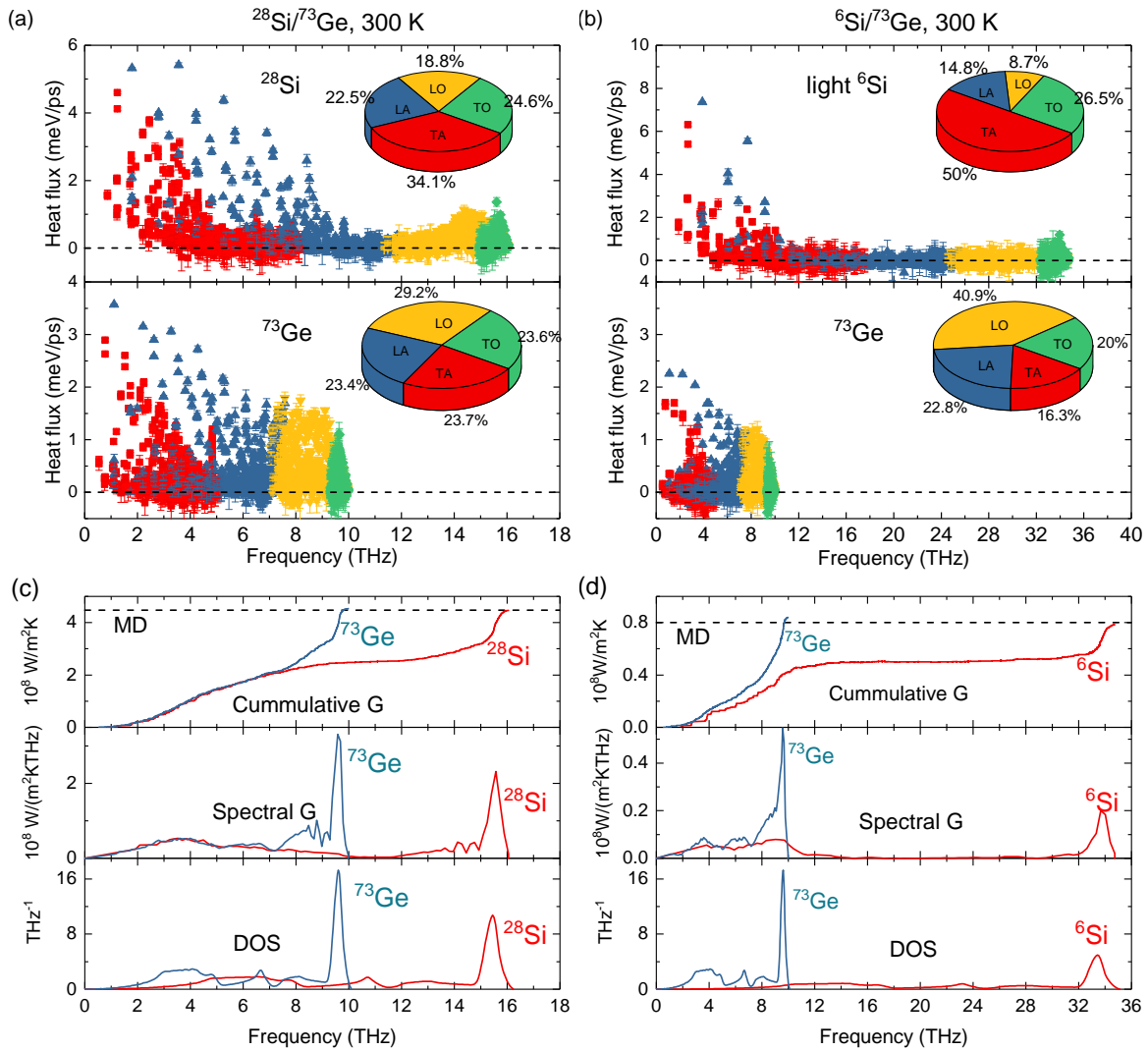


FIG. 4: Modal heat fluxes and conductances for the $^{28}\text{Si}/^{73}\text{Ge}$ and $^6\text{Si}/^{73}\text{Ge}$ interfaces at 300K. The dashed lines are the thermal conductances obtained directly from real space $G = Q_{MD}/\Delta T_{MD}$, where Q_{MD} is rate of the energy injected in the hot reservoir or extracted from the cold reservoir.

flux) generally decay with increasing frequency. The acoustic phonons near the BZ boundary have near-zero conductance. It is generally believed that optical phonons may not contribute much to the interfacial thermal conductance. For example, the widely-used acoustic mismatch model (AMM) only considers acoustic phonons. However, we find that the optical phonons contribute at least 35% to G in all the cases we studied. It is again benefited from the bridging effect of the interfacial modes^{37,38}.

Based on Fig. 4 (a), acoustic phonons dominate the heat flux in Si while optical phonons dominate Ge. Enlarging the mass difference can further increase the significance of the acoustic phonons in Si and the optical phonons in Ge. In other words, the increase of mass difference increases the significance of the energy transfer channel from the low-frequency phonons in Si to the high-frequency phonons in Ge.

We can compare the thermal conductance per mode to gain

insight into the branch contribution. Note that the total number of transverse modes are double of that of longitudinal modes. Therefore, from the pie charts in Figs.4 and 5, it is seen that the longitudinal phonons have much larger thermal conductance per mode than transverse phonons. This result agrees qualitatively with what have been observed in graphene/Si and graphene/graphene systems⁴². In graphene/Si system, the ZA mode in graphene as well as the LA and LO modes in Si dominate the heat transfer. In graphene/graphene overlap junction system, the ZA mode dominates. In all these systems, the phonon modes that vibrate along the heat transfer direction dominate the heat transfer. It can be understood that these modes can directly compress and stretch the lattice along the heat transport direction to transfer energy across interface.

The sign of large inelastic transmission across Si/Ge interface was also observed in literature^{29,37,38}. For example, Chalopin and Volz have observed large transmission coeffi-

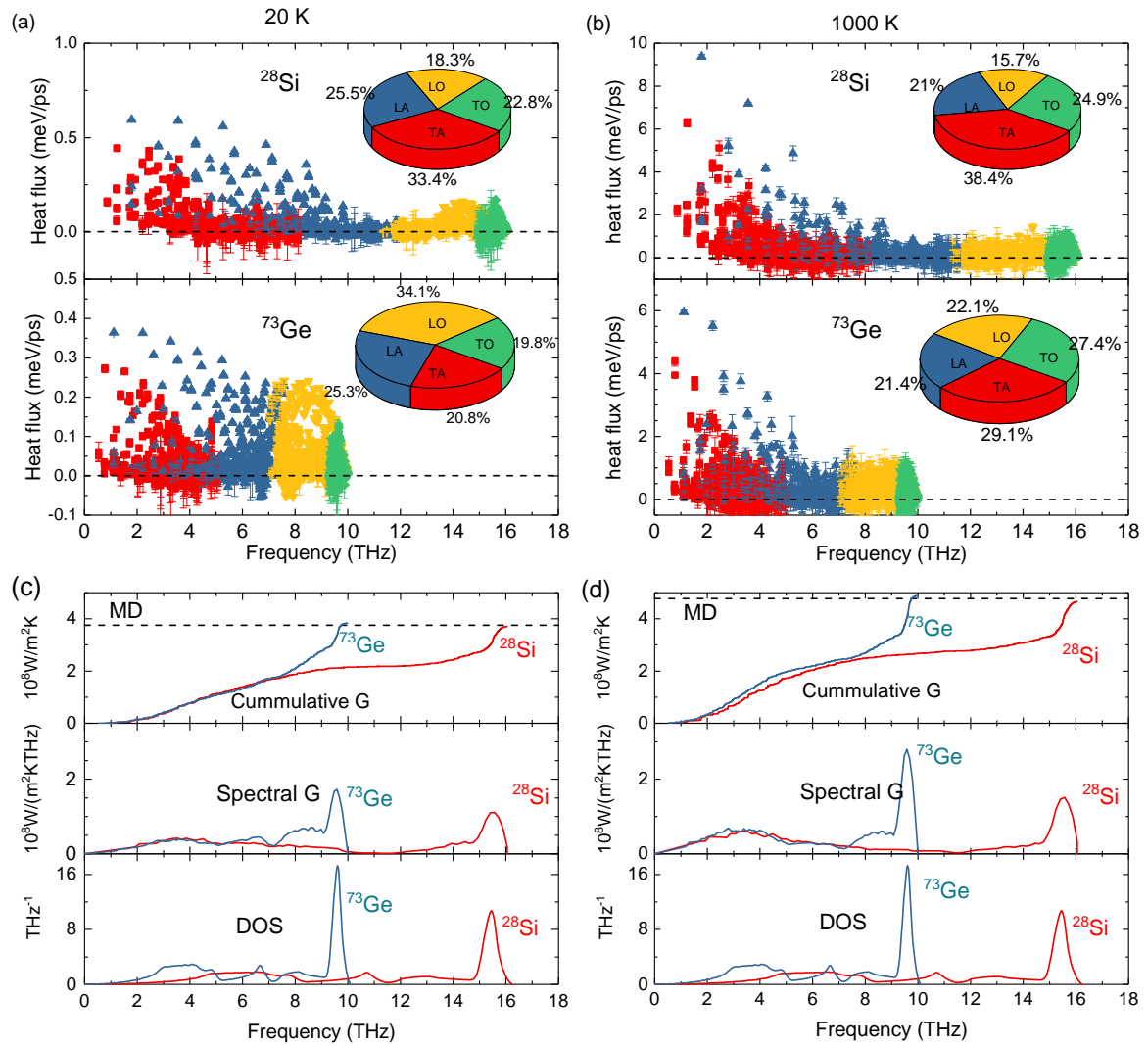


FIG. 5: Modal heat fluxes and conductances for the $^{28}\text{Si}/^{73}\text{Ge}$ interface at 20 and 1000 K.

cient above Ge cutoff frequency for Si/Ge/Si sandwich structure based on equilibrium molecular dynamics. Gordiz and Henry have observed a 10~20% and 50% contributions above Ge cutoff frequency for lattice mismatched and matched cases, respectively^{37,38}. Although their results might be similar to ours, the underlying mechanisms are different. First, the physical meanings are different as discussed in Sec.II C. Second, since equilibrium molecular dynamics were used in their cases, the phonon local nonequilibrium effect near the interface that is presented in real case is not presented in their simulations. This would lead to difference to interfacial thermal transport. Third, as discussed in Sec.I, the coherence effect, which may increase the thermal conductance, for their cases might be strong when periodic boundary condition is applied along the direction of heat flow.

B. Modal temperatures and thermal nonequilibrium

As indicated by Feng *et al.*⁴², the phonons that transport across 2D/2D interface, 2D/2D junction and 2D/3D interface are usually in thermal nonequilibrium. Here, we investigate the modal temperature across the 3D/3D interface, with the results showing in Fig.6 (a). It can be clearly seen that phonons are in large thermal nonequilibrium near the interface, which could be originated from two possible mechanisms. The first is the size effect as indicated by Ref.⁴². In this work the size effect has been largely eliminated as discussed in Sec.II B. Although it might still have some influence to the nonequilibrium somehow, the more important mechanism is the second one, i.e., the existing of interface. The phonons that pass through the interface more easily can gain energy from other phonons by scattering. As a result, their temperatures become higher. Even with infinite-long Si and Ge (completely no size effect), the phonons near the interface will still be in large thermal nonequilibrium.

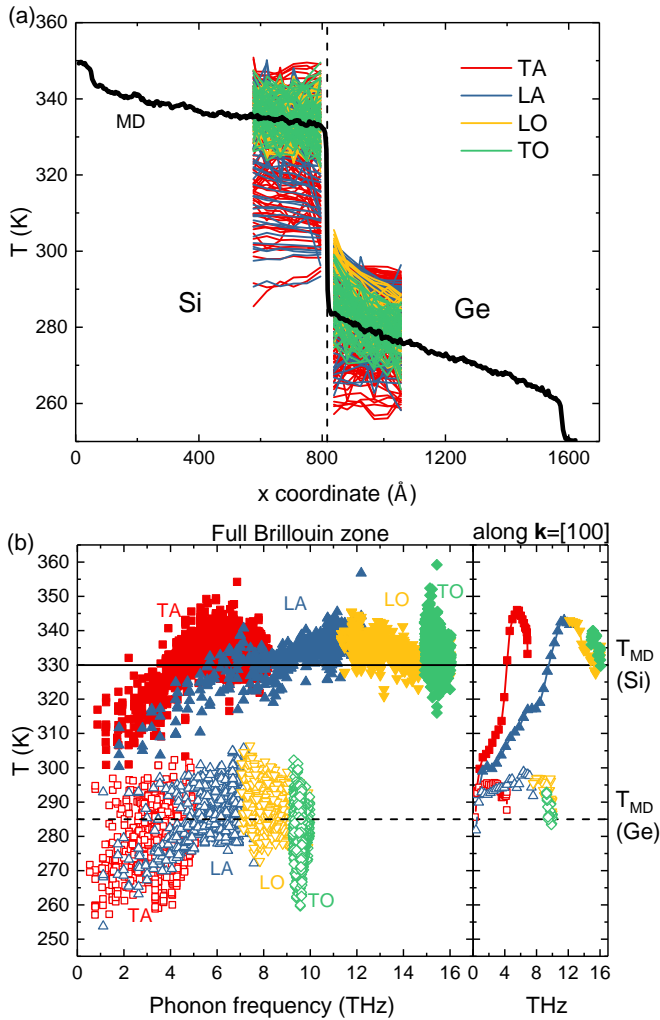


FIG. 6: Phonon temperatures in Si and Ge near the interface as a function of (a) the x coordinate and (b) frequency. In (b), the left panel shows the phonons in the full BZ, and the right panel shows the phonons traveling parallel to x , the direction of heat flow. Solid and open dots represent Si and Ge, respectively. The horizontal solid and dashed lines are the MD temperatures of Si and Ge near the interface, respectively.

The temperatures near interface as a function of frequency are shown in Fig.6 (b). The phonons of silicon are shown as solid dots, and those of germanium open dots. Different branches are differentiated by colors. We find that the phonons are in large thermal nonequilibrium. Instead of staying at the average MD temperature 330 K, the phonons of silicon stay at different temperature spreading from 300 K to 355 K. Similarly, those in Ge spread from 255 to 305 K, deviating from the average MD temperature 285 K.

The phonon local nonequilibrium can impede heat flow. Due to the nonequilibrium, the effective heat carriers (acoustic phonons) have much smaller temperature jump at the interface than what they should have in equilibrium. Therefore, the heat they carry is much smaller than what they should carry in equilibrium. The ineffective heat carriers (optical phonons)

have much larger temperature jump than what they should have in equilibrium, but the heat they carry is not much larger since they are ineffective heat carriers. The overall effect is that the non-equilibrium reduces the effective heat carriers' conductance and enhances the ineffective heat carrier's conductance. A simple math can show that the total heat flux is reduced compared to equilibrium. This effect was actually discussed in literature. For example, it has been shown from both theory⁶⁴ and experiment⁶⁵ that the phonon local nonequilibrium exists in graphene and impede the heat flow. In their case, the electrons heat up optical phonons but it takes some time for these hot optical phonons (ineffective heat carriers) to heat up other acoustic phonons (effective heat carriers). As a result, the optical phonons have large temperature gradients while the acoustic phonons do not. Since the former is ineffective heat carrier, although their large temperature gradients are much larger than the overall temperature gradient, it does not help the system to conductor much more heat. In contrast, the acoustic phonons' much smaller temperature gradient significantly reduces the heat conduction of the system as compared what it should have at equilibrium. Here, we take a simple two-phonon model to explain the mechanism. Suppose the acoustic phonon has thermal conductivity κ_a and temperature gradient ∇T , and the optical phonon has κ_o ($\kappa_o < \kappa_a$) and $3\nabla T$. Assume the optical and acoustic phonons have the same number of modes (work for the crystals with 2 basis atoms such as graphene and silicon), the average temperature gradient⁴² is $2\nabla T$. Therefore, for the nonequilibrium case, the heat flux of the system is $\kappa_a \nabla T + 3\kappa_o \nabla T$. If the phonons are in equilibrium, i.e, they both have temperature gradient as $2\nabla T$, the heat flux is $2(\kappa_a + \kappa_o)\nabla T$, which is larger than the one in non-equilibrium. This two-phonon model provides a simple and clear way to tackle the heat flow problems when phonons are in local non-equilibrium and it has been used in literature⁶⁶. The local non-equilibrium exists in not only semiconductor/semiconductor interfaces for phonon/phonon heat transfer, but also metal/semiconductor interfaces for electron/phonon heat transfer⁶⁷⁻⁶⁹. In these cases, the nonequilibrium also impedes heat flow.

The low-frequency TA and LA modes in Si have lower temperatures than the average, while the higher-frequency phonons in Ge have higher temperature than the average. The hot optical phonons in Si transfer their heat to Ge in two ways. The first way is that they dump heat to the cold low-frequency phonons in Si (due to temperature difference), which is then transferred to Ge. The second way is that they directly transfer their heat to Ge inelastically.

In addition to the frequency dependent results, we have also studied the direction dependence. For example, in the right panel of Fig.6, we have inspected the phonons that travel along the $[100]$ (heat flow) direction. We find that most of the phonons in Ge have much higher temperature than average, indicating that these phonons along $[100]$ are more efficient than the phonons in other directions for the interfacial thermal conductance, which is consistent with intuition. Below 1 THz, the phonon temperature of Si is nearly the same as that in Ge, indicating the elastic transmission is nearly 1 in long-wavelength limit. This agree well with Launder and AMM

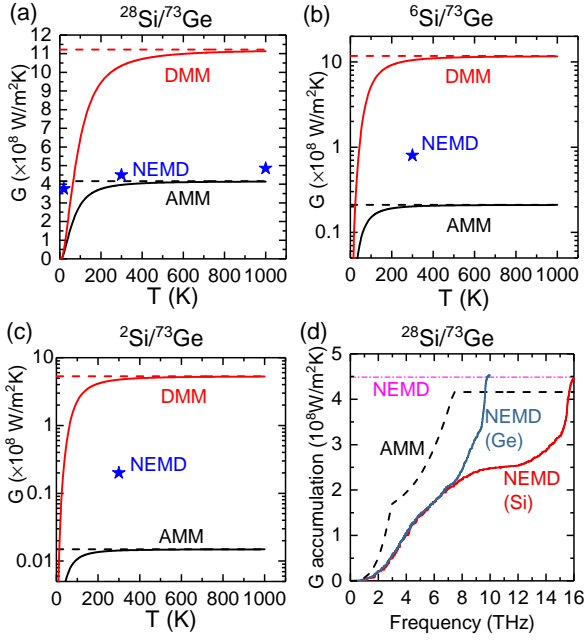


FIG. 7: The comparison between NEMD results with AMM and DMM models. (a) (b) and (c) show the temperature dependent interfacial thermal conductance G for the interfaces of $^{28}\text{Si}/^{73}\text{Ge}$, $^6\text{Si}/^{73}\text{Ge}$ and $^2\text{Si}/^{73}\text{Ge}$, respectively. Black and red represent AMM and DMM, respectively. Solid and dashed lines represent Bose-Einstein and Boltzmann distributions respectively. Blue stars are NEMD results. (d) shows the G accumulation as a function of frequency for $^{28}\text{Si}/^{73}\text{Ge}$ interface at 300 K.

models.

C. Interpretation by modified Landauer approach

It is worth to compare the NEMD results with the widely used AMM and DMM models. We have calculated the thermal conductances of $^{28}\text{Si}/^{73}\text{Ge}$, $^6\text{Si}/^{73}\text{Ge}$ and $^2\text{Si}/^{73}\text{Ge}$ as a function of temperature using AMM and DMM models with Bose-Einstein and Boltzmann distributions. The results are compared to NEMD as shown in Figs.7(a-c). It is seen that the DMM gives much worse results than AMM probably because the interface is planar and clean. Even though the AMM model with Boltzmann distribution predicts well for $^{28}\text{Si}/^{73}\text{Ge}$, its error can grow to be as large as 20 times when the mass difference increases. The reason is that AMM does not include the inelastic transport or the bridging effect of the interfacial modes^{37,38}.

With increasing mass ratio, the relative DMM conductance does not decrease as much as AMM. The reason is that the AMM model assumes mode-to-the-same-mode transmission while DMM does not. For example, AMM assumes that TA of Si can only be transmitted to the TA of Ge, while in DMM, the TA of Si can also be transmitted to TO and LO of Ge. When the mass ratio increases, the total DOS overlap shrinks (DMM conductance decreases as seen in Figs.7), but the overlap between the same mode (for example, the TA in Si and TA in

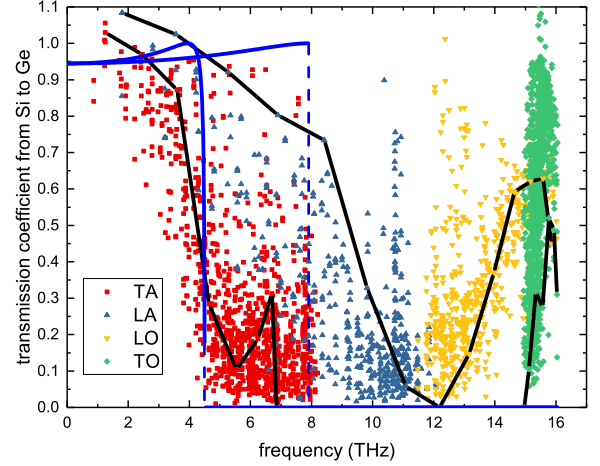


FIG. 8: Transmission coefficients for the modified Landauer approach mapped from NEMD simulations. The dots include all the phonon branches in all incident directions. The black curves pick out the phonons in [100] direction, which propagate towards the interface perpendicularly. The blue curves indicate the transmission coefficients calculated from the AMM model.

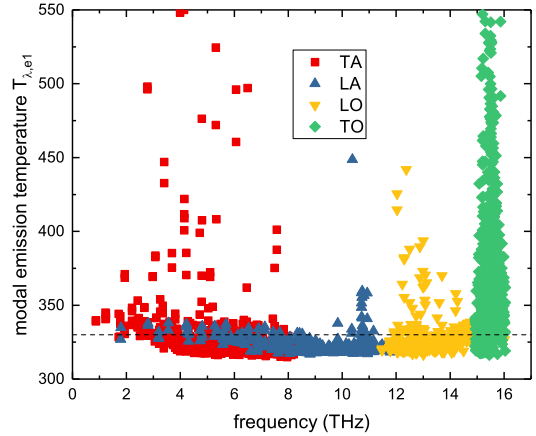


FIG. 9: Modal emission temperatures of silicon. The dashed line indicate the temperature of Si near the interface in NEMD simulations.

Ge) shrinks more significantly (AMM conductance decreases more significantly).

Since the G value of $^{28}\text{Si}/^{73}\text{Ge}$ interface given by the AMM model agrees reasonably well with NEMD, we look into the spectral accumulations to see if they match as well. As shown in Fig.7(d), their G accumulations have large difference. The AMM model assumes thermal equilibrium, which overpredicts the contribution of the low-frequency phonons that are in large nonequilibrium. Furthermore, the AMM model assumes elastic transport and therefore, only the phonons with frequency below 8 THz have contribution to the thermal conductance. In a word, the AMM model may predict well the

G value in some cases coincidentally, but the spectral $G(\omega)$ is still significantly mispredicted.

Although molecular dynamics simulation is more numerically accurate than Landauer approach regarding the inclusion of inelastic transport and phonon nonequilibrium, Landauer approach is widely used because of its clear and simple form and without the need of interatomic potentials which hinder the quantitative comparison to experiments. If the Landauer approach can be revised to include the inelastic and phonon nonequilibrium, it will be of great value to the interfacial thermal transport research. Moreover, studies in literature based on MD and Landauer approaches are conducted separately, but these two methods were not linked yet. Our attempt was to find this link, and our modal NEMD method is ideal for this purpose.

In the following, we modify the Landauer formalism to include the inelastic transmission and modal thermal nonequilibrium:

$$Q_\lambda = \frac{V_{BZ}}{N_{\mathbf{k}}(2\pi)^3} \hbar \omega_\lambda v_\lambda \mathcal{T}_\lambda [f_B(T_{\lambda,e1}) - f_B(T_{\lambda,e2})]. \quad (8)$$

The inclusion of inelastic transmission is realized by modifying the transmission coefficient \mathcal{T}_λ , and the modal nonequilibrium is represented by the modal dependencies of the emission temperatures from left ($T_{\lambda,e1}$) and right ($T_{\lambda,e2}$). In the equation above, V_{BZ} is the volume of Brillouin zone, \hbar is the reduced Planck's constant, ω_λ is the angular frequency of the mode λ , v_λ is the group velocity, and f_B is the phonon population classical distribution – Boltzmann distribution $f_{B,\lambda} = \hbar \omega_\lambda / k_B T_\lambda$.

Based on modified Landauer approach Eq.(8), as long as the transmission coefficient \mathcal{T}_λ and emission temperatures ($T_{\lambda,e1}$ and $T_{\lambda,e2}$) of each phonon mode are known, the modal as well as total heat fluxes can be calculated.

In this work, we do backward calculations, i.e., we use the modal heat flux that was extracted from NEMD simulations to solve the transmission coefficient \mathcal{T}_λ as well as the emission temperatures ($T_{\lambda,e1}$ and $T_{\lambda,e2}$) based on Eq.(8). To solve these three unknowns, we need two more equations, which are listed below. Each mode's temperature T_λ that was extracted from NEMD simulations is related to its two emission temperatures by⁷⁰

$$T_\lambda = T_{e,1} - \frac{1}{2} \mathcal{T}_\lambda (T_{\lambda,e1} - T_{\lambda,e2}). \quad (9)$$

The average emission temperature from two sides is equal to the mean temperature of system:

$$T_{ave,MD} = \frac{1}{2} (T_{\lambda,e1} + T_{\lambda,e2}). \quad (10)$$

Based on Eqs.(8), (9) and (10), the transmission coefficient \mathcal{T}_λ and the emission temperatures ($T_{\lambda,e1}$ and $T_{\lambda,e2}$) are calculated. The transmission coefficients of all the phonon modes propagating towards the interface with all possible angles are shown in Fig. 8. The black curves pick out the phonons propagating towards the [100] direction (perpendicularly towards interface). At low frequency, the acoustic phonons have nearly 100% transmission. The transmission coefficient decreases

with increasing frequency. As the frequency approaches to the maximum of each acoustic branch, the transmission coefficient decreases to zero. Interestingly, owing to inelastic scattering, the LA and optical modes above the cutoff frequency of Ge (10 THz) still have large transmission coefficients. The transmission coefficient data above 1 probably originate from statistical error of MD simulations.

The results are compared to those calculated from AMM model (also in the [100] direction) as depicted by the blue curves. We find that the AMM model eliminates the interbranch transmission, and therefore cuts off the transmission of TA above 4.5 THz and LA above 8 THz. More importantly, it completely cuts off all the optical phonons.

In Fig. 9, the emitted temperatures of all phonon branches are shown as a function of frequency. The dashed line at 330 K indicates the temperature of Si near the interface in NEMD simulations. It is seen that the phonons' emitted temperatures could be much higher or lower. Due to the existence of interface, they are in nonequilibrium.

D. Size effect and reversibility

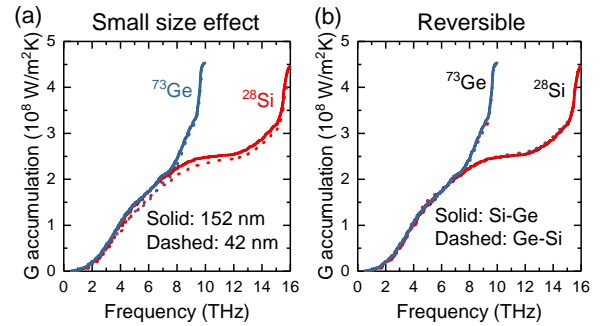


FIG. 10: Interfacial thermal conductance accumulation as a function of frequency for the studies of (a) size effect and (b) reversibility.

It is worth to examine if the size effect has impact on the modal spectral G results, although its impact on the total G value has been eliminated in Sec.II B. The modal $G(\omega)$ accumulations of two different domain sizes of $^{28}\text{Si}/^{73}\text{Ge}$ interface are compared in Fig.10(a). We find that the size effect is small. This is significantly different from homogeneous materials, in which the size effect has large impact on the spectral phonon thermal conductivity⁴².

One more interesting property to examine is the reversibility of the detailed phonon modal transmission processes. For example, in the forward direction from Si to Ge, the high-frequency (>10 THz) phonons in Si cannot pass through the interface elastically since no high-frequency (>10 THz) vibration is allowed in Ge. These phonons have to transfer their heat to the low-frequency phonons in Ge via inelastic scattering. If the heat source and sink are reversed, the low-frequency phonons of Ge can pass through the interface elastically and they do not have to transfer their heat to the high-frequency phonons in Si inelastically. A natural question comes: does the reversed Ge-Si interface have larger elastic and smaller

inelastic thermal transmission than the forward Si-Ge interface? To answer this question, we switch the heat source and sink, and we find that the modal G are identical as shown in Fig.10(b). The result demonstrates that the detailed phonon modal transmission processes are reversible. The thermal rectification cannot be observed in this interface if the temperature difference is not extremely large⁷¹.

IV. CONCLUSIONS

In summary, we have studied a series of Si/Ge interfaces with different mass differences, domain sizes, and temperatures. Surprisingly, we have found that the interfacial modes facilitate the inelastic phonon transport to be larger than 50% of the total thermal conductance. The optical phonons in Si and Ge contribute 43% and 53% to the thermal conductance, respectively. The existence of the interfacial modes' bridging effect can even create effective large four- and five-phonon processes to help the high-frequency phonons to transmit across the interface. We find that the spectral interfacial thermal conductance G follows the shape of phonon DOS, which differentiate significantly from the spectral thermal conductivity

of homogeneous materials. Secondly, we have found large phonon thermal nonequilibrium near the interface, which impedes the thermal conductance of partial phonons. The AMM model cannot predict well the spectral G since it does not consider the thermal nonequilibrium or inelastic transmission. When the mass difference between A and B increases, the AMM model can under-predict the thermal conductance of A/B interface by several to tens of times. We have modified the Landauer approach to include the inelastic transmission and modal thermal nonequilibrium. Last but not least, we find that the detailed elastic and inelastic modal transmissions across interface are reversible. Our results provide a better understanding of the interfacial thermal transport and pave the way to a better control of the interfacial heat flow.

Acknowledgments

Simulations were performed at the Rosen Center for Advanced Computing of Purdue University. The work was supported by the Defense Advanced Research Projects Agency (Award No. HR0011-15-2-0037).

-
- * Electronic address: ruan@purdue.edu
- ¹ N. P. Padture, M. Gell, and E. H. Jordan, *Science* **296**, 280 (2002).
 - ² G. Borman and K. Nishiwaki, *Progress in energy and combustion science* **13**, 1 (1987).
 - ³ E. Pop, *Nano Research* **3**, 147 (2010).
 - ⁴ E. Pop, S. Sinha, and K. E. Goodson, *Proceedings of the IEEE* **94**, 1587 (2006).
 - ⁵ F. Sarvar, D. C. Whalley, and P. P. Conway, in *Electronics System Integration Technology Conference, 2006. 1st* (IEEE, 2006), vol. 2, pp. 1292–1302.
 - ⁶ A. Yu, P. Ramesh, M. E. Itkis, E. Bekyarova, and R. C. Haddon, *The Journal of Physical Chemistry C* **111**, 7565 (2007).
 - ⁷ D. G. Cahill, W. K. Ford, K. E. Goodson, G. D. Mahan, A. Majumdar, H. J. Maris, R. Merlin, and S. R. Phillpot, *Journal of applied physics* **93**, 793 (2003).
 - ⁸ S. T. Huxtable, D. G. Cahill, S. Shenogin, L. Xue, R. Ozisik, P. Barone, M. Usrey, M. S. Strano, G. Siddons, M. Shim, et al., *Nature materials* **2**, 731 (2003).
 - ⁹ W. Little, *Canadian Journal of Physics* **37**, 334 (1959).
 - ¹⁰ E. Swartz and R. Pohl, *Applied Physics Letters* **51**, 2200 (1987).
 - ¹¹ E. T. Swartz and R. O. Pohl, *Reviews of modern physics* **61**, 605 (1989).
 - ¹² W. Zhang, T. Fisher, and N. Mingo, *Numerical Heat Transfer, Part B: Fundamentals* **51**, 333 (2007).
 - ¹³ N. Mingo and L. Yang, *Physical Review B* **68**, 245406 (2003).
 - ¹⁴ W. Zhang, T. Fisher, and N. Mingo, *Journal of heat transfer* **129**, 483 (2007).
 - ¹⁵ Z. Tian, K. Esfarjani, and G. Chen, *Phys. Rev. B* **86**, 235304 (2012), URL <http://link.aps.org/doi/10.1103/PhysRevB.86.235304>.
 - ¹⁶ P. E. Hopkins and P. M. Norris, *Nanoscale and Microscale Thermophysical Engineering* **11**, 247 (2007).
 - ¹⁷ P. E. Hopkins, *Journal of Applied Physics* **106**, 013528 (2009).
 - ¹⁸ P. E. Hopkins, J. C. Duda, and P. M. Norris, *Journal of Heat Transfer* **133**, 062401 (2011).
 - ¹⁹ R. Prasher, *Applied Physics Letters* **94**, 041905 (2009).
 - ²⁰ P. Reddy, K. Castelino, and A. Majumdar, *Applied Physics Letters* **87**, 211908 (2005).
 - ²¹ S. Shin, M. Kaviani, T. Desai, and R. Bonner, *Physical Review B* **82**, 081302 (2010).
 - ²² S. Volz, *Thermal nanosystems and nanomaterials*, vol. 118 (Springer Science & Business Media, 2009).
 - ²³ S. Sadasivam, N. Ye, J. P. Feser, J. Charles, K. Miao, T. Kubis, and T. S. Fisher, *Phys. Rev. B* **95**, 085310 (2017), URL <https://link.aps.org/doi/10.1103/PhysRevB.95.085310>.
 - ²⁴ P. Schelling, S. Phillpot, and P. Keblinski, *Journal of Applied Physics* **95**, 6082 (2004).
 - ²⁵ C. H. Baker, D. A. Jordan, and P. M. Norris, *Physical Review B* **86**, 104306 (2012).
 - ²⁶ P. Schelling, S. Phillpot, and P. Keblinski, *Applied Physics Letters* **80**, 2484 (2002).
 - ²⁷ N. A. Roberts and D. Walker, *Journal of Applied Physics* **108**, 123515 (2010).
 - ²⁸ J. Shi, J. Lee, Y. Dong, A. Roy, T. S. Fisher, and X. Ruan, *Physical Review B* **97**, 134309 (2018).
 - ²⁹ Y. Chalopin and S. Volz, *Applied Physics Letters* **103** (2013), ISSN 00036951.
 - ³⁰ Y. Chalopin, A. Rajabpour, H. Han, Y. Ni, and S. Volz, *Ann. Rev. Heat Transfer* **17**, 147 (2014).
 - ³¹ K. Sääskilähti, J. Oksanen, J. Tulkki, and S. Volz, *Physical Review B* **90**, 134312 (2014), ISSN 1550235X, 1405.3868, URL <http://arxiv.org/abs/1405.3868>.
 - ³² K. Sääskilähti, J. Oksanen, J. Tulkki, and S. Volz, *Physical Review E* **93**, 1 (2016), ISSN 24700053, 1512.05914.
 - ³³ Y. Zhou and M. Hu, *Physical Review B - Condensed Matter and Materials Physics* **95**, 1 (2017), ISSN 1550235X.
 - ³⁴ T. Murakami, T. Hori, T. Shiga, and J. Shiomi, *Applied Physics Express* **7**, 121801 (2014), ISSN 1882-0778, URL

- <http://stacks.iop.org/1882-0786/7/i=12/a=121801?key=crossref.cfdff0fdfaa637e00229503de5c2fb292>.
- 35 A. Giri, J. L. Braun, and P. E. Hopkins, *Journal of Physical Chemistry C* **120**, 24847 (2016), ISSN 19327455.
 - 36 K. Gordiz and A. Henry, *New Journal of Physics* **17**, 103002 (2015), ISSN 13672630, 1407.6410, URL <http://dx.doi.org/10.1088/1367-2630/17/10/103002>.
 - 37 K. Gordiz and A. Henry, *Journal of Applied Physics* **119**, 015101 (2016), ISSN 0021-8979, URL <http://scitation.aip.org/content/aip/journal/jap/119/1/10.1063/1.4939207>.
 - 38 K. Gordiz and A. Henry, *Scientific reports* **6**, 23139 (2016), ISSN 0021-8979, URL <http://scitation.aip.org/content/aip/journal/jap/119/1/10.1063/1.4939207>.
 - 39 R. J. Hardy, *Physical Review* **132**, 168 (1963).
 - 40 G. Domingues, S. Volz, K. Joulain, and J.-J. Greffet, *Phys. Rev. Lett.* **94**, 085901 (2005), URL <https://link.aps.org/doi/10.1103/PhysRevLett.94.085901>.
 - 41 Y. Chalopin, N. Mingo, J. Diao, D. Srivastava, and S. Volz, *Applied Physics Letters* **101**, 221903 (2012), ISSN 00036951, URL <http://link.aip.org/link/APPLAB/v101/i22/p221903/s1{&jAgg=doi>.
 - 42 T. Feng, W. Yao, Z. Wang, J. Shi, C. Li, B. Cao, and X. Ruan, *Physical Review B* **95**, 195202 (2017), ISSN 2469-9950, 1703.10957, URL <http://arxiv.org/abs/1703.10957>.
 - 43 Y. Wang, H. Huang, and X. Ruan, *Physical Review B* **90**, 165406 (2014), ISSN 1098-0121, URL <http://link.aps.org/doi/10.1103/PhysRevB.90.165406>.
 - 44 Y. Zhou and M. Hu, *Physical Review B* **92**, 195204 (2015), ISSN 1098-0121, URL <http://journals.aps.org/prb/abstract/10.1103/PhysRevB.92.195204>.
 - 45 S. Plimpton, *Journal of Computational Physics* **117**, 1 (1995), ISSN 0021-9991, URL <http://www.sciencedirect.com/science/article/pii/S002199918571039X>.
 - 46 J. Tersoff, *Physical Review B* **39**, 5566 (1989), URL <http://journals.aps.org/prb/abstract/10.1103/PhysRevB.39.5566>.
 - 47 J. Tersoff, *Physical Review B* **41**, 3248 (1990), URL <http://journals.aps.org/prb/abstract/10.1103/PhysRevB.41.3248.2>.
 - 48 N. GrÅynbech-Jensen and O. Farago, *Molecular Physics* **111**, 983 (2013), <https://doi.org/10.1080/00268976.2012.760055>, URL <https://doi.org/10.1080/00268976.2012.760055>.
 - 49 E. Landry and A. McGaughey, *Physical Review B* **79**, 075316 (2009).
 - 50 S. C. Huberman, J. M. Larkin, A. J. H. McGaughey, and C. H. Amon, *Physical Review B* **88**, 155311 (2013), ISSN 1098-0121, URL <http://link.aps.org/doi/10.1103/PhysRevB.88.155311>.
 - 51 L. Sun and J. Y. Murthy, *Journal of Heat Transfer* **132**, 102403 (2010).
 - 52 Y. Chalopin, K. Esfarjani, A. Henry, S. Volz, and G. Chen, *Physical Review B* **85**, 195302 (2012).
 - 53 X. Li and R. Yang, *Physical Review B* **86**, 054305 (2012), ISSN 1098-0121, URL <http://link.aps.org/doi/10.1103/PhysRevB.86.054305>.
 - 54 M. S. Shur, *Handbook series on semiconductor parameters*, vol. 1 (World Scientific, 1996).
 - 55 See Supplemental Material for the video.
 - 56 Z. Liang, K. Sasikumar, and P. Keblinski, *Physical Review Letters* **113**, 065901 (2014), ISSN 0031-9007, URL <http://link.aps.org/doi/10.1103/PhysRevLett.113.065901>.
 - 57 W. Li, J. Carrete, N. A. Katcho, and N. Mingo, *Comp. Phys. Commun.* **185**, 1747âÅ§1758 (2014).
 - 58 M. T. Dove, *Introduction to Lattice Dynamics* (Cambridge University Press, New York, USA, 1993).
 - 59 O. N. Bedoya-Martínez, J.-L. Barrat, and D. Rodney, *Physical Review B* **89**, 014303 (2014), ISSN 1098-0121, URL <http://link.aps.org/doi/10.1103/PhysRevB.89.014303>.
 - 60 J. Turney, A. McGaughey, and C. Amon, *Physical Review B* **79**, 224305 (2009), ISSN 1098-0121, URL <http://link.aps.org/doi/10.1103/PhysRevB.79.224305>.
 - 61 W. Lv and A. Henry, *New Journal of Physics* **18**, 013028 (2016), ISSN 1367-2630, 1503.08178, URL <http://iopscience.iop.org/article/10.1088/1367-2630/18/1/013028>.
 - 62 P. Zhang, P. Yuan, X. Jiang, S. Zhai, J. Zeng, Y. Xian, H. Qin, and D. Yang, *Small* **14**, 1702769 (????), <https://onlinelibrary.wiley.com/doi/pdf/10.1002/sml.201702769>, URL <https://onlinelibrary.wiley.com/doi/abs/10.1002/sml.201702769>.
 - 63 X. Wang and B. Huang, *Scientific Reports* **4**, 6399 (2014), ISSN 20452322.
 - 64 A. K. Vallabhaneni, D. Singh, H. Bao, J. Murthy, and X. Ruan, *Phys. Rev. B* **93**, 125432 (2016), URL <http://link.aps.org/doi/10.1103/PhysRevB.93.125432>.
 - 65 S. Sullivan, A. Vallabhaneni, I. Kholmanov, X. Ruan, J. Murthy, and L. Shi, *Nano Letters* **17**, 2049 (2017), pMID: 28218545, <https://doi.org/10.1021/acs.nanolett.7b00110>, URL <https://doi.org/10.1021/acs.nanolett.7b00110>.
 - 66 M. An, Q. Song, X. Yu, H. Meng, D. Ma, R. Li, Z. Jin, B. Huang, and N. Yang, *Nano Letters* **17**, 5805 (2017), pMID: 28777582, <https://doi.org/10.1021/acs.nanolett.7b02926>, URL <https://doi.org/10.1021/acs.nanolett.7b02926>.
 - 67 Y. Wang, X. Ruan, and A. K. Roy, *Physical Review B* **85**, 205311 (2012), ISSN 1098-0121, URL <http://link.aps.org/doi/10.1103/PhysRevB.85.205311>.
 - 68 Z. Lu, Y. Wang, and X. Ruan, *Physical Review B* **93**, 064302 (2016), ISSN 2469-9950, URL <http://link.aps.org/doi/10.1103/PhysRevB.93.064302>.
 - 69 Y. Wang, Z. Lu, A. K. Roy, and X. Ruan, *Journal of Applied Physics* **119**, 065103 (2016), ISSN 0021-8979, URL <http://scitation.aip.org/content/aip/journal/jap/119/6/10.1063/1.4941347>.
 - 70 J. Shi, X. Yang, T. S. Fisher, and X. Ruan, To be published (????), nonequilibrium Landauer approach for thermal interfaces.
 - 71 Y. Wang, A. Vallabhaneni, J. Hu, B. Qiu, Y. P. Chen, and X. Ruan, *Nano letters* **14**, 592 (2014).